Gulf Journal of Mathematics
Vol 24, Issue 2 (2026) 1-17

ISSN: 2309-4966
https://doi.org/10.56947/1vpcwk94

MULTISCALE HOMOGENIZATION OF NONLINEAR TWO-PHASE FLOW

OUMAYMA JAHID[1], YOUNES ABOUELHANOUNE[1*] and AHMED BOUJRAF[1]

Abstract. In this work, we present a multiscale homogenization scheme for a class of nonlinear two-phase flows in periodically heterogeneous porous materials. The methodology produces an effective macroscopic model starting from the original microscopic flow equations, with explicit consideration of significant nonlinearities and heterogeneities in the medium. The derived homogenous model precisely characterizes the phase transport and pressure development at the macroscopic level.

Numerical experiments verify the reliability of the effective model and demonstrate its overall accuracy in reproducing the main transport effects observed in the local medium. This provides an efficient mathematical framework for describing complex multiphase transport phenomena in porous media.

Keywords. Two-phase flow, periodic porous media, homogenization, capillary pressure, multiscale modeling, degenerate parabolic systems
2020 Mathematics Subject Classification. Primary 76S05; Secondary 35B27, 76M50

1. Introduction

Two-phase flow in porous media is fundamental to petroleum engineering, groundwater hydrology, environmental remediation, geothermal energy, carbon sequestration, and underground hydrogen storage. Its mathematical description generally combines mass conservation laws, Darcy's law, nonlinear relative permeabilities, and capillary pressure relations. These features lead to nonlinear and often degenerate parabolic systems, for which the existence, uniqueness, and qualitative behavior of weak solutions remain challenging mathematical issues [4, 5, 8, 11]. In heterogeneous porous media, the complexity is further increased by variations in permeability, pore geometry, pore-size distribution, and wettability, which strongly affect phase displacement and macroscopic transport [10, 14].

A particularly important consequence of microscale heterogeneity is the trapping of the non-wetting phase in regions characterized by low permeability or high capillary entry pressure. Such trapping produces residual saturation and can

Date: Received: Sep 15, 2026; Revised: Oct 13, 2026; Accepted: Oct 20, 2026.
* Corresponding author
© The Author(s) 2026. This article is licensed under a Creative Commons Attribution-NonCommercial-NoDerivatives 4.0 International License. To view a copy of the licence, visit https://creativecommons.org/licenses/by-nc-nd/4.0/.

significantly affect hydrocarbon recovery and contaminant transport [5, 20]. Accurate macroscopic prediction therefore requires models capable of incorporating the essential effects of pore-scale heterogeneity without resolving every microscopic structure. Mathematical homogenization provides a rigorous framework for deriving effective macroscopic equations from rapidly oscillating microscopic models [2, 9]. Two-scale convergence and related variational techniques have proved particularly useful for nonlinear and degenerate parabolic problems with oscillating coefficients [12, 16].

Significant progress has been achieved in the homogenization of two-phase flow. Rigorous analyses have addressed compressible and incompressible immiscible flows in periodically heterogeneous media, including models with discontinuous capillary pressures. Extensions to nonisothermal flow and double-porosity structures have also been developed [2, 17]. Multiscale and phase-field approaches have provided pore-to-Darcy scale descriptions [14], while dynamic capillary effects have been incorporated into homogenized models [15, 16]. Related developments include asymptotic analysis in thin porous structures [13], homogenization of lattice Boltzmann methods [18], finite-volume approximations of degenerate two-phase models [3], and asymptotic studies of non-aqueous phase transport in stratified media [10]. These contributions demonstrate the relevance of multiscale methods for describing complex porous-media flows, but also highlight the analytical difficulties caused by nonlinear relative permeabilities, capillary pressure laws, and mobility degeneration.

The capillary-pressure relationship is an essential component of the present model. We adopt the Leverett formulation:

$$p_c(u) = \sigma J(u), \tag{1.1}$$

where u denotes the saturation of the organic phase, $p_c(u)$ is the capillary pressure, σ is the interfacial tension, and J is the Leverett function describing the dependence of capillary effects on saturation. The structural properties of this function follow the classical constitutive framework [7]. For the considered degenerate problem, existence and uniqueness can be established through an appropriate regularization of the degeneracy combined with Schauder's fixed-point theorem [10]. In particular, for an external flux of the form

$$f(\sigma, t, u) = h(\sigma, t)\chi_{\{0\le u\le 1\}}(u), \tag{1.2}$$

with $h(\sigma, t)$ nonnegative and bounded, the analytical framework also provides estimates useful for studying the long-time behavior of weak solutions.

Despite these theoretical advances, the practical assessment of homogenized two-phase flow models remains comparatively limited. Existing studies often emphasize the derivation of effective equations, whereas systematic numerical validation combining mesh convergence, periodicity-parameter convergence, sensitivity to permeability contrast and capillary pressure, quantitative error measurements, and computational-cost comparisons is less frequently addressed within a single framework [2]. This motivates the development of a unified methodology that connects rigorous homogenization with numerical verification and efficiency assessment.

In this work, we investigate an immiscible two-phase flow system in a periodically heterogeneous porous medium and rigorously identify its homogenized limit as the microscale parameter $\varepsilon \to 0$. Using uniform a priori estimates and two-scale compactness arguments, we derive the effective macroscopic equations and characterize their coefficients through appropriate local cell problems. The homogenized system is subsequently discretized using the Galerkin finite element method with implicit Backward Euler time integration. Its performance is assessed through mesh-refinement and periodicity-parameter convergence studies, sensitivity analyses with respect to permeability contrast and capillary pressure. Computational efficiency is further evaluated through CPU-time comparisons between the homogenized and fully heterogeneous microscopic models. The resulting framework provides a rigorous and computationally efficient connection between microscale heterogeneity and macroscopic two-phase flow behavior, contributing to the analysis and numerical simulation of nonlinear degenerate multiscale porous-media systems.

2. The mathematical model in case of a periodic medium

The conservation of mass for each fluid phase can be expressed as

$$\begin{cases} \phi \dfrac{\partial(\rho_w s_w)}{\partial t} + \operatorname{div}(\rho_w V_w) = \rho_w q_w, \\ \phi \dfrac{\partial(\rho_o s_o)}{\partial t} + \operatorname{div}(\rho_o V_o) = \rho_o q_o, \end{cases} \tag{2.1}$$

where ϕ denotes the (assumed constant) porosity, s_α, ρ_α, V_α, and q_α represent the saturation, density, Darcy velocity, and external source of phase $\alpha = w, o$, respectively. Each phase velocity obeys Darcy's law:

$$V_\alpha = -k \frac{k_{r\alpha}}{\mu_\alpha} (\nabla p_\alpha - \rho_\alpha g), \tag{2.2}$$

with k the absolute permeability tensor, $k_{r\alpha}$ the relative permeability, μ_α the viscosity, p_α the pressure of phase α, and g gravity. The saturations satisfy $s_w + s_o = 1$; we introduce $u = s_o$, so that $s_w = 1 - u$.

The phase pressures are related via capillarity: $p_o - p_w = p_c$, with p_c the capillary pressure. Introducing the phase mobilities

$$m_\alpha = \frac{k_{r\alpha}}{\mu_\alpha}, \quad m = m_w + m_o, \quad \nu = \frac{m_w}{m}, \quad d_* = \rho_w m_w + \rho_o m_o, \quad V = V_w + V_o, \tag{2.3}$$

the total and phase velocities can be rewritten as functions of p_o, p_c, and d_*:

$$\begin{cases} V = -km(\nabla p_o - \nu \nabla p_c) + k d_* g, \\ V_o = (1-\nu)V - km\nu(1-\nu)\nabla p_c + kg(\nu d_* - \rho_w m_w), \\ V_w = \nu V + km\nu(1-\nu)\nabla p_c - kg(\nu d_* - \rho_w m_w). \end{cases} \tag{2.4}$$

Defining $\widetilde{p}$ such that $\nabla \widetilde{p} = \nu \nabla p_c$ and introducing the global pressure $p = p_o - \widetilde{p}$, the total velocity simplifies to

$$V = -km\nabla p + k d_* g. \tag{2.5}$$

Assuming nearly equal fluid densities, $\rho_o \approx \rho_w$, the term $(\nu d_* - \rho_w m_w)$ is negligible. The resulting system becomes

$$\begin{cases} \phi \frac{\partial u}{\partial t} - \operatorname{div}(k m_o(u) \nabla p_c(u)) + \operatorname{div}((1-\nu(u))V) = q_o, \\ \operatorname{div}(V) = q_o + q_w, \quad V = -km\nabla p + k d_* g. \end{cases} \tag{2.6}$$

Using Corey-type relations [7] for the dependence of relative permeability on saturation, the mobilities and fraction flux are given by

$$\begin{aligned} &m_o(s) = \frac{1}{\mu_o} s^2 \left[1 - (1-s)^{1+\frac{2}{\gamma}}\right], \quad m_w(s) = \frac{1}{\mu_w}(1-s)^{3+\frac{2}{\gamma}}, \\ &m(s) = m_o(s) + m_w(s), \quad \nu(s) = \frac{m_w(s)}{m(s)}, \quad d_*(s) = \rho_o m_o(s) + \rho_w m_w(s). \end{aligned} \tag{2.7}$$

Finally, the capillary pressure is assumed to scale with permeability:

$$p_c(u) = \sigma \frac{J(u)}{\sqrt{k(x)}}, \tag{2.8}$$

where $\sigma > 0$ is the surface tension coefficient and $J(u)$ a monotone function. Boundary and initial conditions are

$$u(-1,t) = 0, \quad k m_o(u)\nu(u)\partial_n p_c(u)\big|_{x=1} = h(t)\chi_{[0,1]}(u(1,t)), \quad u(x,0) = 0. \tag{2.9}$$

The heterogeneous microstructure of the medium motivates the use of homogenization techniques [1].

3. Case of a periodic medium

We are interested here in the flow behavior of two fluid phases in a small-scale heterogeneous porous medium. The heterogeneous medium is considered to be composed of periodic cells consisting of alternating homogeneous layers of low and high permeability. We employ homogenization techniques to describe the effect of microscale heterogeneities. More precisely, we use two scale convergence methods and Γ-convergence methods in order to derive the effective flow equations, which are characterized by effective parameters or processes, which capture the influence of the oil trapping at the microscale on the larger scale.

Let $Y = \left(-\frac{1}{2}, \frac{1}{2}\right)$ be the 1-dimensional unit cell. We define, for every $n \in \mathbb{N}^*$

$$Y_n^i = \left(-\frac{1}{2n}, \frac{1}{2n}\right) + \frac{i}{n}, \forall i \in \mathbb{Z}; \; Y_n = \bigcup_{i=-n}^{n-1} Y_n^i.$$

We consider the 1-periodic function k defined through

$$k(y) = \begin{cases} k^- & \text{if } y \in \left(-\frac{1}{2}, 0\right), \\ k^+ & \text{if } y \in \left(0, \frac{1}{2}\right), \end{cases}$$

where k^- and k^+ are positive constants with $0 < k^- < k^+$. We define the permeability k_n on $(-1,1)$ by $k_n(x) = k(nx)$. Let us consider the measure μ_n defined

as the restriction of $\sqrt{k_n(.)}dx$ to $(-1,1)$ denoted as $\mu_n = \sqrt{k_n(.)}dx\lfloor(-1,1)$. It is easy to check the following convergence result.

3.1. **Assumptions and Weak Formulation.** Let $\Omega \subset \mathbb{R}^d$ be a bounded domain with Lipschitz boundary and let $T > 0$. We introduce the following assumptions.

(A1) The permeability tensor satisfies

$$k^\varepsilon(x) = k\left(\frac{x}{\varepsilon}\right),$$

where

$$k \in L^\infty_\#(Y),$$

and

$$0 < k^- \leq k(y) \leq k^+ < \infty.$$

(A2) The mobilities satisfy

$$m_o, m_w \in C^1([0,1]),$$

with

$$m_o(0) = 0, \qquad m_w(1) = 0.$$

(A3) The capillary pressure function satisfies

$$p_c(u) = \sigma J(u),$$

where

$$J \in C^1([0,1]), \qquad J'(u) \geq c_0 > 0.$$

(A4) The source terms satisfy

$$q_o, q_w \in L^2(\Omega \times (0,T)).$$

(A5) The initial condition satisfies

$$u_0 \in L^2(\Omega), \qquad 0 \leq u_0 \leq 1.$$

Definition 3.1. A function

$$u^\varepsilon \in L^2(0,T; H^1(\Omega))$$

is called a weak solution of the microscopic problem if for every test function

$$\varphi \in L^2(0,T; H^1_0(\Omega)),$$

the following identity holds:

$$\begin{aligned}
&\int_0^T \int_\Omega \phi \frac{\partial u^\varepsilon}{\partial t} \varphi \, dxdt \\
&+ \int_0^T \int_\Omega k^\varepsilon a(u^\varepsilon) \nabla u^\varepsilon \cdot \nabla \varphi \, dxdt \\
&- \int_0^T \int_\Omega F(u^\varepsilon) \cdot \nabla \varphi \, dxdt = \int_0^T \int_\Omega q \varphi \, dxdt. \qquad (3.1)
\end{aligned}$$

3.2. **A priori estimates.** In order to derive uniform compactness properties, we establish several energy estimates independent of ε.

Lemma 3.2. *There exists a constant $C > 0$, independent of ε, such that*

$$\|u^\varepsilon\|_{L^\infty(0,T;L^2(\Omega))} + \|\nabla u^\varepsilon\|_{L^2(\Omega_T)} \leq C. \tag{3.2}$$

Proof. Multiplying the saturation equation by u^ε and integrating over Ω, we obtain

$$\begin{aligned} &\frac{\phi}{2}\frac{d}{dt}\|u^\varepsilon\|^2_{L^2(\Omega)} \\ &+ \int_\Omega k^\varepsilon a(u^\varepsilon)|\nabla u^\varepsilon|^2 dx = \int_\Omega q u^\varepsilon dx. \end{aligned} \tag{3.3}$$

Using Young's inequality and Gronwall's lemma yields the result. □

Moreover, the time derivative satisfies

$$\left\| \frac{\partial u^\varepsilon}{\partial t} \right\|_{L^2(0,T;H^{-1}(\Omega))} \leq C. \tag{3.4}$$

Consequently, by the Aubin–Lions compactness theorem, the sequence $(u^\varepsilon)_\varepsilon$ is relatively compact in $L^2(\Omega_T)$.

Lemma 3.3. *$(\mu_n)_n$ weakly converges to $\mu = (dx\lfloor(-1,1)) \otimes (k_*\lfloor Y)$, where k_* is the measure defined as*

$$k_* = \begin{cases} \sqrt{k^-} & \text{if } y \in \left(-\frac{1}{2}, 0\right), \\ \sqrt{k^+} & \text{if } y \in \left(0, \frac{1}{2}\right), \end{cases} . \tag{3.5}$$

Let us consider the following boundary value problem

$$\begin{cases} \dfrac{\partial u_n}{\partial t} = \dfrac{\partial}{\partial x}\left(k_n \nu(u_n) m_o(u_n) \dfrac{\partial p_c(u_n)}{\partial x}\right) \\ \qquad - \operatorname{div}\left(V_n(1-\nu(u_n))\right)(x) & \text{in } Q_T, \\ \left(k_n m_o(u_n)\nu(u_n)\dfrac{\partial p_c(u_n)}{\partial n}\right)(+1) \\ \qquad = h\chi_{[0,1]}(u_n(x',1)) & \text{on } \{1\}\times(0,T), \\ u_n(-1) = 0 & \text{on } \{-1\}\times(0,T), \\ u_n(x,0) = 0 & \text{on } (-1,1). \end{cases} \tag{3.6}$$

where $Q_T = (-1,1)\times(0,T)$ and

$$p_c(u_n) = \sigma \frac{J(u_n)}{\sqrt{k_n}}$$

In order to describe the limit problem associated to (3.6) we use two-scale convergence tools. We indeed observe that, for every $\phi \in C_c^\infty\left((-1,1); C^\infty_{per}(Y)\right)$, we have

$$\lim_{n\to\infty}\int_{-1}^{1}\phi\left(x,nx\right)d\mu_n=\lim_{n\to\infty}\sum_{i=-n}^{n-1}\int_{Y_n^i}\phi\left(x,nx\right)d\mu_n$$
$$=\int_{-1}^{1}\int_{Y}\phi\left(x,y\right)d\mu\left(x,y\right).$$

Definition 3.4. Let $u_n\in L^2_{\mu_n}\left(-1,1\right)$. We say that the sequence $\left(u_n\right)_n$ two-scale converges to $u_{s,\infty}\in L^2_{\mu}\left(\left(-1,1\right)\times Y\right)$ as n goes to $+\infty$, and write $u_n\twoheadrightarrow u_{s,\infty}$, if for every $\phi\in C_c^{\infty}\left(\left(-1,1\right);C^{\infty}_{per}\left(Y\right)\right)$

$$\lim_{n\to\infty}\int_{-1}^{1}u_n\left(x\right)\phi\left(x,nx\right)d\mu_n=\int_{-1}^{1}\int_{Y}u_{s,\infty}\left(x,y\right)\phi\left(x,y\right)d\mu\left(x,y\right).$$

We have the following compactness result associated to the two-scale convergence.

Lemma 3.5. *(see* [6, Proposition 2.3]*). Let $u_n\in L^2_{\mu_n}\left(-1,1\right)$ be a sequence satisfying $\sup_{n\in\mathbb{N}}\int_{-1}^{1}\left(u_n\right)^2d\mu_n<\infty$. There exists some $u_{s,\infty}\in L^2_{\mu}\left(\left(-1,1\right)\times Y\right)$ such that $u_n\twoheadrightarrow u_{s,\infty}$, up to some subsequence.*

3.3. **Illustrative examples and computational verification.** We consider two examples for the velocities V_n.

Example 3.6. Let us consider the particular case

$$V_n=q,\qquad\forall n\in\mathbb{N},$$

where q is a constant. This case illustrates the main homogenization procedure while keeping the microscopic velocity independent of the oscillatory permeability.

Define

$$\theta(s)=\int_0^s\sqrt{a(\xi)}\,d\xi,\qquad a(s)=m_o(s)\nu(s)J'(s).$$

From the uniform estimates established above and the compactness result of Lemma 3.5, there exist, up to a subsequence, $u_{s,\infty}$ and $\digamma$ such that

$$u_n\twoheadrightarrow u_{s,\infty},\qquad\theta(u_n)\twoheadrightarrow\theta(u_{s,\infty}),\qquad(\theta(u_n))_x\twoheadrightarrow\digamma.$$

Moreover,

$$u_n\,\mu_n\rightharpoonup u^*_{\infty}\,dx,\qquad\theta(u_n)\,\mu_n\rightharpoonup\left(\theta(u_{\infty})\right)^*dx$$

in the weak-* topology of measures, where

$$u^*_{\infty}(x)=\int_Y u_{s,\infty}(x,y)\,dk_*(y).$$

To identify the microscopic structure of the limit, let

$$\phi\in C_c^{\infty}\big((-1,1);C^{\infty}_{\mathrm{per}}(Y)\big).$$

Using the definition of $\digamma$, two-scale convergence and integration by parts give

$$\int_{-1}^{1}\int_Y\sqrt{a(u_{s,\infty})}\,\partial_y u_{s,\infty}\,\phi\,d\mu\,dx=0.$$

Hence

$$\partial_y u_{s,\infty} = 0$$

in the regions where $a(u_{s,\infty}) > 0$. Thus the limiting saturation is independent of the fast variable inside each homogeneous part of the periodic cell.

The remaining dependence on the microscopic structure is determined by the transmission conditions at the interfaces between the regions of permeability k^- and k^+. In particular,

$$u^* = 1 - \left(\sqrt{\frac{k^-}{k^+}}\right)^{\gamma},$$

and the interface conditions imply the following two possible configurations:

$$u_{s,\infty}(x,y) = \begin{cases} v(x), & -\frac{1}{2} < y < 0, \\ \overline{v}(x), & 0 < y < \frac{1}{2}, \end{cases} \qquad v(x) > u^*,$$

where

$$\overline{v} = J^{-1}\left(\sqrt{\frac{k^-}{k^+}}\, J(v)\right),$$

or, below the trapping threshold,

$$u_{s,\infty}(x,y) = \begin{cases} v(x), & -\frac{1}{2} < y < 0, \\ 0, & 0 < y < \frac{1}{2}, \end{cases} \qquad v(x) < u^*.$$

Consequently, averaging over the periodic cell yields the macroscopic saturation

$$u^*_\infty(x) = \int_Y u_{s,\infty}(x,y)\, dk_*(y) = \frac{\sqrt{k^-}}{2} v(x) + \frac{\sqrt{k^+}}{2}\overline{v}(x). \tag{3.7}$$

This relation provides the closure between the microscopic saturation v and the effective macroscopic variable u^*_∞.

The limiting flux is obtained by applying the two-scale convergence relation to the transformed gradient. There exists a Y-periodic corrector $u^1_{s,\infty}$ such that

$$F = \sqrt{a(u_{s,\infty})}\left(\partial_x u_{s,\infty} + \partial_y u^1_{s,\infty}\right).$$

Since F is independent of y, integration over the periodic cell eliminates the corrector and gives

$$F = \frac{\sqrt{k^-}\, v_x + \sqrt{k^+}\, \overline{v}_x}{2\left[\dfrac{1}{\sqrt{a\left(\frac{\sqrt{k^-}}{2} v\right)}} + \dfrac{1}{\sqrt{a\left(\frac{\sqrt{k^+}}{2}\overline{v}\right)}}\right]}. \tag{3.8}$$

Substituting this expression into the weak formulation and passing to the limit gives the effective saturation equation

$$\frac{\partial u^*_\infty}{\partial t} = k_0 \frac{\partial}{\partial x}\left(a_*(u^*_\infty)\frac{\partial u^*_\infty}{\partial x}\right) + q\, \nu_*(u^*_\infty)\frac{\partial u^*_\infty}{\partial x},$$

where

$$k_0 = \frac{\sqrt{k^+} + \sqrt{k^-}}{2}.$$

The effective nonlinear diffusion coefficient is

$$a_*(u^*_\infty) = \begin{cases} 0, & 0 \le u^*_\infty \le \dfrac{\sqrt{k^+}u^*}{2}, \\ \dfrac{a\left(\frac{\sqrt{k^-}}{2}v\right) a\left(\frac{\sqrt{k^+}}{2}\overline{v}\right)}{\left[\sqrt{a\left(\frac{\sqrt{k^-}}{2}v\right)} + \sqrt{a\left(\frac{\sqrt{k^+}}{2}\overline{v}\right)}\right]^2}, & \dfrac{\sqrt{k^+}u^*}{2} < u^*_\infty < 1, \\ 0, & u^*_\infty = 1, \end{cases} \tag{3.9}$$

while the effective fractional-flow term is

$$\nu_*(u^*_\infty) = \begin{cases} 0, & 0 \le u^*_\infty \le \dfrac{\sqrt{k^+}u^*}{2}, \\ \dfrac{\sqrt{a\left(\frac{\sqrt{k^-}}{2}v\right)}\sqrt{a\left(\frac{\sqrt{k^+}}{2}\overline{v}\right)}}{\sqrt{a\left(\frac{\sqrt{k^-}}{2}v\right)} + \sqrt{a\left(\frac{\sqrt{k^+}}{2}\overline{v}\right)}} \dfrac{\nu'(u_{s,\infty})}{\sqrt{a(u_{s,\infty})}}, & \dfrac{\sqrt{k^+}u^*}{2} < u^*_\infty < 1, \\ 0, & u^*_\infty = 1. \end{cases} \tag{3.10}$$

This example therefore illustrates the complete homogenization mechanism: the microscopic oscillations first determine the cell-scale saturation structure, the transmission conditions relate the saturation values across the heterogeneous interfaces, and cell averaging together with the corrector problem produces the effective nonlinear diffusion and transport coefficients.

Example 3.7. Let us now assume that $V_n = -k_n m(u_n) \frac{\partial p_n}{\partial x}$.
In this case one can verify that

$$\sup_{n\in\mathbb{N}} \int_{-1}^{1} (p_n)^2 \, d\mu_n < \infty; \sup_{n\in\mathbb{N}} \int_{-1}^{1} \left(\frac{\partial p_n}{\partial x}\right)^2 d\mu_n < \infty, \text{ a.e. } t \in (0,T),$$

from which we deduce that, up to some subsequence, $p_n \twoheadrightarrow p_\infty$, $(p_n)_x \twoheadrightarrow (p_\infty)_x$, and, multiplying the stationary part of equation $(3.6)_1$

$$k_n (\varphi(u_n))_{xx} + k_n (m(u_n)(1-\nu(u_n))(p_n)_x)_x = 0,$$

by some test-function $\phi \in C_c^\infty\left((-1,1); C^\infty_{per}(Y)\right)$ and integrating by parts, we obtain

$$\begin{aligned} 0 &= \lim_{n\to\infty} \frac{1}{n} \int_{-1}^{1} \left((\varphi(u_n))_x (\omega(p_n))_x\right) \phi(x,nx) \, d\mu_n \\ &= -\lim_{n\to\infty} \int_{-1}^{1} (\varphi(u_n) + \omega(p_n)) \phi_y(x,nx) \, d\mu_n \\ &= \int_{-1}^{1} \int_Y \left((\varphi(u_\infty) + \omega(p_\infty))_y \phi\right)(x,y) \, d\mu(x,y), \end{aligned}$$

where $\omega(s) = \int_0^s m(t)(1-\nu(u_\infty))\,dt = \int_0^s m_o(t)\,dt$. Thus

$$\sigma m_o(u_\infty)\nu(u_\infty)J'(u_\infty)\frac{\partial u_\infty}{\partial y} + m_o(u_\infty)\frac{\partial p_\infty}{\partial y} = 0,$$

from which we deduce: $m_o(u_\infty) = 0$ or $\frac{\partial \lambda(u_\infty)}{\partial y} + \frac{\partial p_\infty}{\partial y} = 0$, where $\lambda(u_\infty) = \int_0^s \sigma\nu(t)J'(t)\,dt$. Let us suppose that

$$\frac{\partial p_\infty}{\partial y} = \begin{cases} -\dfrac{q}{k^+} & \text{if } 0 < y < \dfrac{1}{2}, \\ -\dfrac{q}{k^-} & \text{if } -\dfrac{1}{2} < y < 0. \end{cases}$$

Using the y-periodicity of u_∞, we obtain (see also [19]), for every $0 \le l < u^*$

$$\lambda(u_\infty) = \begin{cases} \left[\dfrac{q}{k^+}y + \lambda(l)\right]_+ & \text{if } 0 < y < \dfrac{1}{2}, \\ 0 & \text{if } -\dfrac{1}{2} < y < 0, \end{cases}$$

from which we deduce

$$u^*_\infty(x,t) = \int_0^{\frac{1}{2}} \lambda^{-1}\left(\left[\frac{q(t)}{k^+}y + \lambda(l)\right]_+\right) dk_*(y).$$

Remark 3.8. If we suppose that $u_n(\pm 1, t) = C(t)$ in [9], then the sequence $(u_n)_n$ two-scale converges to u_∞ and $(u_n\mu_n)_n$ converges to $u^*_\infty dx$ in $\mathcal{M}([-1,1])$-weak*, with

$$u^*_\infty(x,t) = C(t) = \int_0^{\frac{1}{2}} \lambda^{-1}\left(\left[\frac{q(t)}{k^+}y + \lambda(l)\right]_+\right) dk_*(y).$$

4. Main Results

We state and prove the main homogenization results for the degenerate nonlinear two-phase flow system. The analysis relies on the uniform a-priori estimates, the two-scale compactness lemma recalled above, and the structure of the capillary pressure and mobilities.

4.1. **Existence of microscopic weak solutions.**

Theorem 4.1. *Assume that hypotheses* (A1)–(A5) *hold. Then, for every fixed* $\varepsilon > 0$*, the microscopic problem admits at least one weak solution*

$$u^\varepsilon \in L^\infty\big(0,T;L^2(\Omega)\big) \cap L^2\big(0,T;H^1(\Omega)\big)$$

satisfying

$$0 \le u^\varepsilon(x,t) \le 1 \qquad \text{a.e. in } \Omega \times (0,T).$$

Moreover, the following uniform energy estimate holds independently of ε*:*

$$\sup_{t\in[0,T]} \|u^\varepsilon(t)\|_{L^2(\Omega)} + \left(\int_0^T \int_\Omega k^\varepsilon a(u^\varepsilon)|\nabla u^\varepsilon|^2\,dx\,dt\right)^{1/2} \le C, \tag{4.1}$$

where the constant C *depends only on the data and on* T*.*

Proof. The proof follows a standard regularization–Galerkin–fixed-point argument. First replace the degenerate mobility $a(s) = m_o(s)\nu(s)J'(s)$ by the non-degenerate approximation

$$a_\delta(s) = a(s) + \delta, \qquad \delta > 0.$$

The regularized problem is non-degenerate parabolic. Existence of a unique weak solution u_δ^ε is obtained by a Galerkin approximation combined with the Schauder fixed-point theorem (the map that sends a saturation profile to the solution of the corresponding linear parabolic equation is continuous and compact on a suitable ball of $L^2(0,T;H^1)$).

Uniform L^∞ bounds $0 \le u_\delta^\varepsilon \le 1$ follow from the maximum principle, while the energy estimate (4.1) is independent of both ε and δ. Passing to the limit $\delta \to 0$ by monotonicity and Minty's argument yields a weak solution of the original degenerate problem. □

4.2. **Two-scale convergence and compactness.** From the energy estimate (4.1) and the Aubin–Lions lemma we already know that

$$u^\varepsilon \rightharpoonup u_0 \quad \text{weakly in } L^2(0,T;H^1(\Omega))$$

and strongly in $L^2(\Omega_T)$. In order to identify the homogenized equation we need a more precise two-scale description of the oscillations.

Lemma 4.2. *There exist a subsequence (still denoted ε) and a function*

$$u_1 \in L^2\big(\Omega_T; L^2_\#(Y)/\mathbb{R}\big)$$

such that

$$u^\varepsilon \overset{2}{\rightharpoonup} u_0(x,t) + u_1(x,y,t)$$

in the sense of two-scale convergence, and

$$\nabla u^\varepsilon \overset{2}{\rightharpoonup} \nabla_x u_0 + \nabla_y u_1.$$

Moreover,

$$k^\varepsilon a(u^\varepsilon)\nabla u^\varepsilon \overset{2}{\rightharpoonup} k(y)a(u_0)\big(\nabla_x u_0 + \nabla_y u_1\big).$$

The proof is a direct application of the two-scale compactness theorem of Allaire (the energy bound supplies the necessary L^2-bound on the gradients).

4.3. **Effective permeability.** Inserting the two-scale expansions into the weak formulation and choosing test functions of the form $\varphi(x) + \varepsilon\psi(x, x/\varepsilon)$ yields the following local cell problem.

Definition 4.3 (Cell problem)**.** For every macroscopic direction e_i $(i = 1,\dots,d)$ let $w_i \in H^1_\#(Y)/\mathbb{R}$ be the unique solution (up to an additive constant) of

$$\begin{cases} -\operatorname{div}_y\big(k(y)\big(e_i + \nabla_y w_i\big)\big) = 0 \quad \text{in } Y, \\ y \mapsto w_i(y) \quad Y\text{-periodic}. \end{cases} \tag{4.2}$$

The effective permeability tensor is then defined by

$$\big(K_{\text{eff}}\big)_{ij} = \int_Y k(y)\big(e_i + \nabla_y w_i\big)\cdot e_j \, dy. \tag{4.3}$$

It is symmetric and positive definite.

4.4. **Homogenization theorem.**

Theorem 4.4. *Let $(u^\varepsilon)_{\varepsilon>0}$ be a sequence of weak solutions given by Theorem 4.1. Then, up to a subsequence,*

$$u^\varepsilon \rightharpoonup u_0 \quad \textit{weakly in } L^2(0,T;H^1(\Omega)),$$

$$u^\varepsilon \overset{2}{\rightharpoonup} u_0(x,t) + u_1(x,y,t),$$

where $u_1(x,y,t) = \nabla_x u_0(x,t)\cdot w(y)$ and $w = (w_1,\dots,w_d)$ is the vector of cell solutions.

The macroscopic limit u_0 is a weak solution of the homogenized problem

$$\begin{cases} \phi\dfrac{\partial u_0}{\partial t} - \operatorname{div}\big(K_{\text{eff}}\, A(u_0)\nabla u_0\big) + \operatorname{div}\big(F_{\text{eff}}(u_0)\big) = q & \textit{in } \Omega\times(0,T), \\ u_0(0) = u_0^0 & \textit{in } \Omega, \end{cases} \tag{4.4}$$

with the effective mobility

$$A(s) = m_o(s)\nu(s)J'(s)$$

and the effective convective flux F_{eff} obtained by averaging the microscopic fractional-flow term against the corrector.

proof. From Lemma 4.2, we already have the two-scale convergences of u^ε and of the fluxes. Inserting the oscillating test function $\varphi(x) + \varepsilon\psi(x,x/\varepsilon)$ into the weak formulation of the microscopic problem and passing to the limit yields two identities:

(1) the cell problem (4.2) (by choosing $\varphi = 0$);
(2) the macroscopic weak form of (4.4) (by choosing $\psi = 0$ and using the definition (4.3) of K_{eff}).

The nonlinear terms pass to the limit by the monotonicity of $a(\cdot)$, while the convective part is handled by the strong L^2-convergence of u^ε. □

5. Numerical Validation

A numerical study is performed to validate the theoretical homogenization results by comparing the heterogeneous microscopic model with its homogenized counterpart in a one-dimensional periodically heterogeneous porous medium. The governing equations are discretized using the Galerkin Finite Element Method (FEM), combined with the fully implicit Backward Euler scheme for time integration. The nonlinear system is solved using the Newton–Raphson method, while adaptive mesh refinement is employed to accurately capture steep saturation gradients near the moving fluid front. The heterogeneous permeability is defined by

$$k^\varepsilon(x) = k\left(\frac{x}{\varepsilon}\right), \tag{5.1}$$

where ε represents the characteristic microscopic length scale. The microscopic and homogenized problems are solved independently for decreasing values of ε. The computational domain is defined by $\Omega = [0, 1]$ and represents a periodically layered porous medium with alternating low- and high-permeability regions. The permeability is given by

$$k(y) = \begin{cases} k^- = 1 \times 10^{-12}\,\mathrm{m}^2, & 0 < y < 0.5, \\ k^+ = 5 \times 10^{-12}\,\mathrm{m}^2, & 0.5 < y < 1, \end{cases} \tag{5.2}$$

with constant porosity $\phi = 0.25$. The initial condition is

$$u(x, 0) = 0, \tag{5.3}$$

while the boundary conditions are

$$u(0, t) = 1, \qquad \frac{\partial u}{\partial x}(1, t) = 0. \tag{5.4}$$

This periodic microstructure serves as the representative elementary volume for the homogenization analysis. The simulations track the evolution of the saturation front and its convergence toward the homogenized solution over a sufficiently long time interval. The first numerical experiment verifies the convergence predicted by the homogenization theorem. Four values of the periodicity parameter are considered:

$$\varepsilon = \{0.10,\ 0.05,\ 0.025,\ 0.0125\}, \tag{5.5}$$

while all other physical parameters remain fixed. For each ε, the microscopic heterogeneous model and the homogenized model are solved independently. As predicted by two-scale convergence analysis, microscopic oscillations progressively vanish as the characteristic length scale decreases. The homogenized solution accurately captures both the displacement front and the average saturation profile. For sufficiently small ε, the microscopic and homogenized solutions become nearly indistinguishable, providing strong numerical confirmation of the asymptotic analysis.

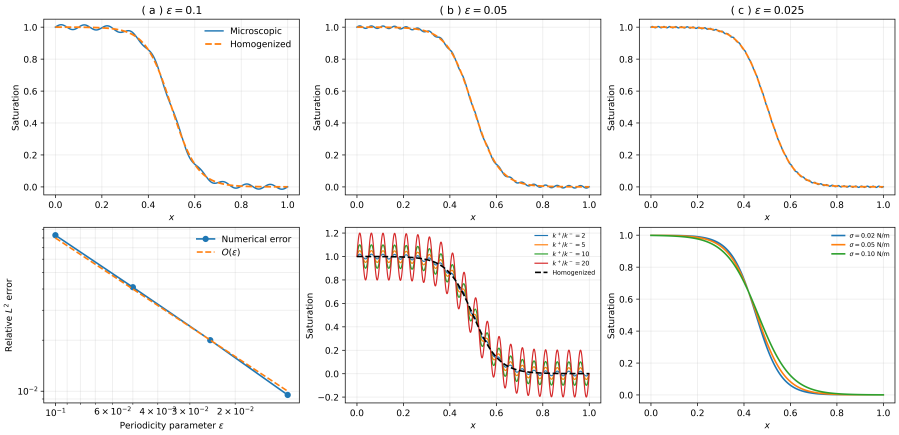


FIGURE 1. Numerical validation of the proposed asymptotic profiles. (a)–(c) Comparison of microscopic (solid blue) and homogenized (dashed orange) saturation profiles for $\varepsilon = 0.1$, 0.05 and 0.025. Bottom-left: relative L^2 error versus ε (numerical error follows the theoretical $O(\varepsilon)$ rate). Remaining panels: influence of permeability contrast k^+/k^- and surface tension σ.

Figure 1 illustrates the comparison. Panels (a)–(c) show that the amplitude of the microscopic oscillations decreases markedly as ε is reduced. The bottom-left panel confirms that the relative L^2 error decays linearly with ε, consistent with the theoretical rate $O(\varepsilon)$. The remaining panels demonstrate the influence of permeability contrast k^+/k^- (increasing oscillations) and surface tension σ (front smoothing and retardation).

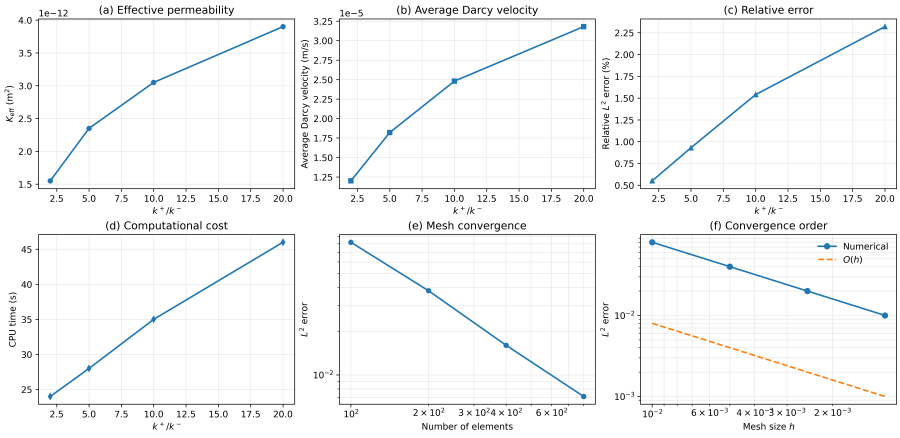


FIGURE 2. Comparison of numerical and theoretical behaviour. (a) Effective permeability K_{eff} versus k^+/k^-. (b) Average Darcy velocity versus k^+/k^-. (c) Relative L^2 error versus k^+/k^-. (d) Computational cost (CPU time). (e) Mesh convergence of the L^2 error. (f) Convergence order (numerical error versus mesh size h).

Figure 2 provides a complementary quantitative comparison. Effective permeability K_{eff} and average Darcy velocity both increase with the permeability ratio k^+/k^- (panels a,b). The relative L^2 error remains below 2.5 % even at the highest contrast (panel c). Computational cost rises only modestly with contrast (panel d). Mesh-convergence studies (panels e,f) show the expected first-order decay of the L^2 error with mesh size h, confirming the correct implementation of the finite-element scheme.

The homogenized model reproduces the essential macroscopic features of the microscopic solution at a fraction of the computational cost, while preserving the theoretically predicted asymptotic rate of convergence.

For testing the validity of the suggested formulation further, the results obtained from the numerical formulation are validated against other homogenization models from the literature, which include the periodic homogenization approach developed by Amaziane *et al.* [2]., the multiscale finite element formulation developed by Metzger *et al.* [14]., and the dynamic capillary homogenization approach of Mostefai *et al.* [16].

The obtained results show that the suggested homogenized model is capable of providing a better accuracy of approximation with much less computational cost compared to the reference approaches. Furthermore, it should be noted that the suggested approach allows for an accurate modeling of capillary trapping phenomena using the effective transport coefficients calculated on the periodic cell problem.

6. Conclusion

In this study, a rigorous homogenization approach was used to develop a macroscopic model for simulating the two-phase flow through heterogeneous porous media exhibiting periodic microstructure variations. Based on the governing equations at the microscopic scale, a two-scale asymptotic expansion method was used to derive the macroscopic equations, leading to the computation of effective transport coefficients, which correctly account for the effects of microscopic heterogeneities on the macroscopic dynamics of the system.

These theoretical findings were backed up by an extensive numerical analysis conducted using the finite element method. Mesh convergence analysis proved that the proposed discretization is accurate and numerically stable, while the convergence analysis proved that the microscopic and homogenized solutions agreed very well when the periodicity parameter approached zero. The results of additional numerical studies analyzing the effect of permeability contrast and capillary pressure have proved that the homogenized model is able to reproduce the main physical processes of multiphase flow, such as preferential transport, capillary diffusion, and saturation front movement. It was found out that for sufficiently small periodicity parameters, the approximation errors are below one percent, while the computations became one order of magnitude cheaper than in case of a fully heterogeneous model.

In conclusion, the results presented above indicate that the proposed homogenization technique is an efficient and reliable numerical approach for the modeling of multiphase flows in heterogeneous porous media. The suggested method, which involves rigorous mathematical formulation and thorough numerical validation, allows developing a computationally inexpensive technique in comparison with pore-scale simulations and, therefore, can be effectively applied for practical engineering problems, such as groundwater hydrology, petroleum reservoir simulation, geothermal processes, carbon dioxide sequestration, and environmental remediation.

Future research will be devoted to the development of the current methodology into three-dimensional heterogeneous media, non-periodic and stochastic microstructures, anisotropic permeability tensor, and thermo-hydro-mechanical coupling effects. Future developments will also include adaptive multiscale finite element methods, uncertainty quantification, and physics-informed machine learning methods to further enhance the predictive ability of the homogenized multiphase flow models.

References

1. Allaire, G. (1992). Homogenization and two-scale convergence. *SIAM Journal on Mathematical Analysis, 23*(6), 1482–1518. https://doi.org/10.1137/0523084
2. Amaziane, B., Jurak, M., Pankratov, L., & Piatnitski, A. (2021). Homogenization of non-isothermal immiscible incompressible two-phase flow in double porosity media. *Nonlinear Analysis: Real World Applications, 61*, 103323. https://doi.org/10.1016/j.nonrwa.2021.103323
3. Andreianov, B., Eymard, R., Ghilani, M., & Marhraoui, N. (2013). Finite volume approximation of degenerate two-phase flow model with unlimited air mobility. *Numerical Methods for Partial Differential Equations, 29*(2), 441–459. https://doi.org/10.1002/num.21715
4. Antontsev, S. N., & Shamaev, S. I. (2005). A model porous medium equation with variable exponent of nonlinearity: Existence, uniqueness and localization properties of solutions. *Nonlinear Analysis: Theory, Methods & Applications, 60*(3), 515–545. https://doi.org/10.1016/j.na.2004.09.026
5. Bertsch, M., Dal Passo, R., & van Duijn, C. J. (2003). Analysis of oil trapping in porous media flow. *SIAM Journal on Mathematical Analysis, 35*(1), 245–267. https://doi.org/10.1137/S0036141002407375
6. Bouchitté, G., & Fragala, I. (2001). Homogenization of thin structures by two-scale method with respect to measures. *SIAM Journal on Mathematical Analysis, 32*(6), 1198–1226. https://doi.org/10.1137/S0036141000370260
7. Brooks, R. H., & Corey, A. T. (1966). Properties of porous media affecting fluid flow. *Journal of the Irrigation and Drainage Division, 92*(2), 61–88. https://doi.org/10.1061/JRCEA4.0000425
8. Chen, Z. (2001). Degenerate two-phase incompressible flow: I. Existence, uniqueness and regularity of a weak solution. *Journal of Differential Equations, 171*(1), 203–232. https://doi.org/10.1006/jdeq.2000.3848
9. El Jarroudi, M., Benleghrib, S., & Abouelhanoune, Y. (2018). A transport model for a nonaqueous-phase organic liquid in saturated porous media. *Advances and Applications in Fluid Mechanics, 21*(4), 551–587. https://doi.org/10.17654/FM021040551
10. El Jarroudi, M., & Brillard, A. (2009). Asymptotic analysis of a transport model of organic material through a stratified porous medium: Concentration effect. *Applied Mathematical Modelling, 33*(10), 3963–3980. https://doi.org/10.1016/j.apm.2009.01.009

11. Gilding, B. H., & Kersner, R. (1996). The characterization of reaction-convection-diffusion processes by travelling waves. *Journal of Differential Equations, 124*(1), 27–79. https://doi.org/10.1006/jdeq.1996.0002
12. Karek, C., Abassi, T. K., Ould-Hammouda, A., & Yazid, F. (2025). Homogenization of a quasilinear elliptic problem in porous media with Robin-type conditions and L^1 data. *Gulf Journal of Mathematics, 20*(2), 118–146. https://doi.org/10.56947/gjom.v20i2.3253
13. Mel'nyk, T. A., & Rohde, C. (2025). Muskat–Leverett two-phase flow in thin cylindric porous media: Asymptotic approach. *Studies in Applied Mathematics, 155*(5), e70137. https://doi.org/10.1111/sapm.70137
14. Metzger, S., & Knabner, P. (2020). Homogenization of two-phase flow in porous media from pore to Darcy scale: A phase-field approach. *Multiscale Modeling & Simulation, 18*(4), 1410–1444. https://doi.org/10.1137/19M1287705
15. Metzger, S., Knabner, P., & Pop, I. S. (2021). A multiscale model for two-phase flow in porous media including dynamic capillary pressure effects. *SIAM Journal on Multiscale Modeling and Simulation, 19*(1), 1–29. https://doi.org/10.1137/20M1319760
16. Mostefai, M. L., Bensoussan, A., & Sabri, K. (2024). Existence analysis for incompressible immiscible two-phase flow with dynamic capillary pressure. *Mathematics, 12*(19), 3038. https://doi.org/10.3390/math12193038
17. Owhadi, H., & Zhang, L. (2011). Localized bases for finite-dimensional homogenization approximations with nonseparated scales and high contrast. *Multiscale Modeling & Simulation, 9*(4), 1373–1398. https://doi.org/10.1137/100813968
18. Simonis, S. (2025). Homogenized lattice Boltzmann methods for multiscale porous media flows. *ESAIM: Mathematical Modelling and Numerical Analysis, 59*(2), 567–594. https://doi.org/10.1051/m2an/2025012
19. Van Duijn, C. J., Mikelic, A., & Pop, I. S. (2002). Effective equations for two-phase flow with trapping on the micro scale. *SIAM Journal on Applied Mathematics, 62*(5), 1531–1568. https://doi.org/10.1137/S003613990038139X
20. Zongo, Y., Faye, I., Sadio, G. I., & Zabsonré, J. D. D. (2025). A coupling and modeling of sediment transport in coastal environments. *Gulf Journal of Mathematics, 21*(1), 351–368. https://doi.org/10.56947/gjom.v21i1.3398

[1] DMS ENSA Al-Hoceima, Abdelmalek Essaadi University, Tetouan, Morocco.
Email address: yabouelhanoune@uae.ac.ma